Generic rules of lumen nucleation and fusion in epithelial organoids

Linjie Lu[†1-4], Kana Fuji[†5], Tristan Guyomar[1-4], Michèle Lieb[1-4], Sakurako Tanida[5-7], Makiko Nonomura[8], Tetsuya Hiraiwa[9,10, 5], Yara Alcheikh[12], Siham Yennek[11], Heike Petzold[12], Cecilie Martin-Lemaitre[13], Anne Grapin-Botton*[12,14], Alf Honigmann*[12-14], Masaki Sano*[15,5], Daniel Riveline*[1-4]

[1]Institut de Génétique et de Biologie Moléculaire et Cellulaire, Illkirch, France
[2]Université de Strasbourg, Illkirch, France
[3]Centre National de la Recherche Scientifique, UMR7104, Illkirch, France
[4]Institut National de la Santé et de la Recherche Médicale, U964, Illkirch, France
[5]Universal Biology Institute, Graduate School of Science, The University of Tokyo, Tokyo, Japan
[6]Research Center for Advanced Science and Technology, The University of Tokyo, Tokyo, Japan
[7]Department of Aeronautics and Astronautics, School of Engineering, The University of Tokyo, Tokyo, Japan
[8]Department of Mathematical Information Engineering, College of Industrial Technology, Nihon University, Chiba, Japan
[9]Mechanobiology Institute, Singapore, National University of Singapore, Singapore
[10]Institute of Physics, Academia Sinica, Taipei, Taiwan
[11]The Novo Nordisk Foundation Center for Stem Cell Biology, Copenhagen, Denmark
[12]Max Planck Institute of Molecular Cell Biology and Genetics, Dresden, Germany
[13]Technische Universität Dresden, Biotechnologisches Zentrum, Center for Molecular and Cellular Bioengineering (CMCB), Dresden, Germany
[14]Cluster of Excellence Physics of Life, TU Dresden, 01062 Dresden, Germany
[15]Institute of Natural Sciences, School of Physics and Astronomy, Shanghai Jiao Tong University, Shanghai, China

[†]Joint first authors
***Corresponding authors: botton@mpi-cbg.de, alf.honigmann@tu-dresden.de, sano.masaki@sjtu.edu.cn, and riveline@unistra.fr**

Abstract: Many internal organs in the body harbor a fluid-filled lumen. The mechanisms of lumens initiation and fusion have been reported as dependent on organ-type during organogenesis. In contrast, the physics of lumen suggests that force balance between luminal pressure and cell mechanics could lead to conserved rules which may unify their self-organisation. However, this hypothesis lacks experimental evidence. Here we show that lumens share similar dynamics for three different systems (MDCK cysts, pancreatic spheres, and epiblast cysts) by using quantitative cell biology, microfabrication and theory. We report that initial cell number determines the maximum number of lumens but does not impact the steady state which is a final single lumen. In addition, lumens numbers exhibit two phases over time, a nucleation phase followed by a fusion phase. In the nucleation phase, lumens form between two cells in pancreatic and MDCK cysts whereas they form at the rosette stage between ten cells in epiblasts. In the second phase, lumens fuse by an increase in lumen volume for pancreatic spheres and MDCK cysts, whereas cell convergent directional motion leads to lumens fusion in epiblasts. We support these results by reproducing numerically lumens dynamics using a phase field model with simple rules for cell proliferation, cell adhesion and lumen growth. We finally use MDCK cysts to manipulate cell adhesion and lumen volume and we successfully reproduce the fusion dynamics of pancreatic spheres and epiblasts. Our results reveal self-organisation rules of lumens across systems with relevance for morphogenesis during development and for the design of synthetic organs.

Introduction.

Physical properties of cells and tissues cross-talk with genetic and molecular control to set the rules for morphogenesis[1,2]. Organogenesis relies on individual cells that proliferate and interact to self-organise. The cells in different organs use common modules controlling cell division, cell volume and shape, cell rearrangement and migration to enable different shapes to emerge[3] . Basic physical parameters of cells such as pressure differences or surface tension are crucial in the process. A physics treatment of organogenesis aims to be generic and applicable to different cell types.

We took this generic approach to study the dynamics of a central structure in organs, *i.e.,* the lumen which forms in epithelial organ models. It was reported that several mechanisms of lumen formation are conserved across mutliple systems such as hollowing after cell division[4–8] or by apoptosis leading to cavitation[7–9]. In addition, theory for the physics of lumen was proposed[10,11] and some physical mechanisms for its dynamics were reported experimentally[12,13]. However, a systematic comparison between cellular systems is lacking so far. Here, we probed self-organisation of lumens on *in vitro* models. We use epithelial organoids as paradigms for lumen dynamics with physiological relevance[14,15].

To determine the rules of self-organisation of lumens, we used organotypic MDCKII cells modeling kidney tubule, pancreatic spheres modeling pancreatic ducts and (mouse Embryonic Stem Cell) mESC-derived epiblast organoids modeling the early steps of epiblast lumen formation. To enable quantitative comparisons and reproducibility we imposed the initial cell numbers for our three cellular systems. This was controlled by plating cells in microfabricated cavities designed to contain the specific targeted cell number. We followed the number of lumens as a function of time for each system. We report that they present the same trend, *i.e.,* an increase in the number of lumens as a function of time (Phase 1) followed by a decrease due to fusion (Phase II) until they all reach a single lumen. We also show that MDCKII and pancreatic spheres nucleate lumens either after cell division or upon cell contact whereas epiblasts form lumens when they reach a rosette stage of 10 cells. In contrast, fusion of lumens is dominated by increase in pressure for pancreatic and MDCK spheres, whereas epiblast lumens fuse by cell motion. These generic rules are substantiated with a numerical simulation reproducing cell dynamics and lumen appearance using a phase field approach. To further test these mechanisms, we used MDCK cysts to manipulate adhesion and lumen volume and we successfully reproduce the fusion dynamics of pancreatic spheres and epiblasts.

Results.

To track the growth and morphology of organoids (Fig. 1), we designed a microwell-containing device optimized for cell imaging and cyst tracking by using soft lithography[16] (Fig. 1a and Materials and Methods). Single devices contained microwells of different diameters adjusted to the measured mean cell dimension of each cellular system and a constant height equal to the cell height (Ext. Fig. 1). This allowed us to follow different initial cell numbers over time within the same experiment, *i.e.,* 1, 2, 3, 4, 8, 16 cells (Fig. 1c). We used an MDCK cell line which expressed markers for cell-cell junctions and for lumens (see Materials and Methods) and this allowed us to track in three dimensions the number of lumens as a function of time (Fig. 1b-e). We observed two phases, Phase I with an increase in the number of lumens during the first 24 hours followed by Phase II with a decrease over time eventually reaching a single lumen. This suggests that cells formed new lumens over time and that these lumens underwent fusion irrespectively of their initial number. These lumens could also undergo fusion irrespectively of their initial number during Phase II. In addition, larger initial cell numbers correlated to larger number of lumens,

ranging from a peak of 1 lumen for 1 initial cell at 24 hours to 6 lumens on average for 16 initial cells. They reached single lumen within 24 hours (1 day) for 1 initial cell and 192 hours (8 days) for 16 initial cells.

We further explored whether this biphasic behavior was conserved in other systems. We plated pancreatic cells freshly isolated from fetal mouse pancreases at 13.5 days of development in the micro-cavities with adjusted dimensions and we tracked the evolution of lumen number over time (Fig. 2a and Fig. 2b). We quantified these dynamics (Fig. 2b) and we found a biphasic trend similar to the MDCK system (Fig. 1e). However, the distribution ranged from a peak of 1 lumen for 1 initial cell at 16 hours to 5 lumens on average for 16 initial cells. Lumens fused into a single lumen within 24 hours and 48 hours respectively. The same experiment with epiblasts led to similar conclusions (Fig. 2c and Fig. 2d): the lumen numbers increased and then decreased reaching single lumens, ranging from a peak of 1 lumen to 4 lumens on average for 1 cell and 16 cells initial cell numbers. Lumen fusion into a single lumen happened within 2 days and 3 days respectively. Altogether all systems exhibited the same qualitative behavior, increase in lumen number with increasing initial cell numbers, and an increase of lumens number followed by fusion leading to single lumens.

The three systems exhibited similar phases but with a different timing. We hypothesized that this may be due to different cell cycle lengths of the different cell types. We thus plotted the number of lumens per cell cycle as a function of initial cell number for each system (Fig. 3a). Remarkably, the curves were similar for MDCK cysts and pancreatic spheres with an increase of 0.2 lumen per cell cycle per initial cell number. In contrast, the slope was 5 times smaller for epiblasts, suggesting differences in the nucleation mechanisms. Following the dynamics of MDCK cells we could see that lumens formed by two mechanisms (Fig. 3b and Movie 1). As described previously, cells nucleated a lumen in the middle of the cell-cell contact after cell division[6,17] (see time 1:40 top Fig. 3b). In addition, we found that two cells formed a lumen when they adhered to each other (see time 2:00 bottom Fig. 3b and Movie 2). The time needed for lumen appearance was similar between both processes (Fig. 3c). Both mechanisms were also observed in pancreatic cells (Fig. 3d, Movie 3 and Movie 4) with the same typical 2 hours timescale to nucleate a lumen (Fig. 3e). It is worth noting that the low number of lumens per cell cycle per initial cell number suggests that lumens are nucleated during this Phase I but also undergo fusion with other lumens. The mechanism of nucleation was in sharp contrast with the appearance of lumens in the epiblasts (Fig. 3f and Fig. 3g): the lumen nucleated only when a critical number of about 10 cells formed a rosette (see time 48h in Fig. 3f and Fig. 3g). This may explain the distinct dynamics in Phase I.

The decrease in lumen number seen over time in Phase II suggested that lumen disappeared by lumen fusion (Fig. 4a). Live imaging enabled us to observe and quantify lumen fusion. We plotted the lumen fusion per cell cycle as a function of initial cell number (Fig. 4a). Unlike for Phase I, the three systems exhibited different fusion slopes. The fusion was the fastest in pancreatic spheres with a decrease of 0.1 per cell cycle per initial cell number, followed by the epiblasts with a decrease of 0.08 per cycle per initial cell number. In contrast the decrease was about 3 times smaller for MDCK lumens fusions than for the other organoids. To further compare the systems, we followed the dynamics of fusion of cysts for initial conditions of 8 cells until cysts reached similar dimensions and cell numbers (Fig. 4b). MDCK cysts exhibited a striking dynamic: the nearest neighbouring lumens coming to contact fused by breaking the cellular junctions separating them over 60 hours (Fig. 4b and Movie 5). We quantified these dynamics by plotting the lumen index (LI) per lumen; LI quantifies the ratio between the luminal area and outer cyst area to capture the respective increase in lumen volume (Fig. 4c, see Materials and Methods). The LI of one lumen increased whereas the LI of the neighbouring lumens decreased in the period preceding the

fusion. This sequence of events was similar for pancreatic sphere fusion but with faster kinetics (Fig. 4b and Movie 6). This was also seen in the LI quantification (Fig. 4d). In contrast, when we tracked the fusion of epiblasts lumens (Fig. 4b and Movie 7) we did not see a significant increase in the LI as illustrated by a constant LI prior fusion (Fig. 4e). The large LI close to 1 for pancreatic sphere may suggest that the luminal pressure is larger than the MDCK sphere which presents a lumen index of 0.3 which is 3 times larger than the epiblast LI. This indicates that increase in luminal pressure is large and important in pancreatic and in MDCK spheres. If pressure is a driver of fusion, we reasoned that it must rip apart the adhesion between cells separating two lumens. To gain insight into adherens junctions, we quantified the levels of E-cadherins levels at junctions (see Ext. Fig. 3c). The mean concentration of E-cadherin was much larger for MDCK spheres compared to the other systems, which suggests that adhesion force may counteract lumen fusion via luminal pressure in this system. This feature may explain the lower slope for the lumen fusion for MDCK cysts compared to pancreatic spheres which may be dominated by large luminal pressure and low adhesion (Fig. 4a).

Since the slope of lumen fusion was much lower for MDCK cysts than pancreatic spheres and epiblasts, we sought for an alternative mechanism driving lumen fusion. The lumen index value of epiblasts suggests that luminal pressure does not play a key role in the fusion. In particular the neighbouring rosettes compacted into a sphere in epiblasts (Fig. 4b) and this was associated to the transformation of the outer layer of the cyst from an elongated shape to a sphere (Fig. 4i) in contrast to MDCK fusion case where the cyst remained spherical (Fig. 4f). We then measured the distance gained along the long axis of the cyst by cells: they corresponded to the distance needed for the lumens to fuse (Fig. 4j,k, see Materials and Methods). This is in sharp contrast with MDCK cysts (Fig. 4g,h). These experiments suggest that lumens fusion in epiblasts are driven by cells convergent directional motion associated with changes in cyst shape, whereas lumens fusions are mainly mediated by luminal pressure for MDCK cysts and pancreatic spheres.

We turned to numerical simulations to reveal the rules in cell proliferation, cell adhesion, lumen formation and luminal pressure, which could reproduce the main results across systems. These *in silico* experiments enabled us to test the hypotheses derived from our observations. In this context, we selected the phase field model which captures the dynamics of cells and lumens[18–20]. We assumed that cells grow and divide at threshold time and volume and form a lumen (Fig. 5a) and we modulate the increase in lumen volume and control cell-cell adhesion (see Suppl. Note Theory). We illustrate typical evolutions of the numerical cysts with 8 cells as initial cell number with the knowledge of the respective proliferation time of our systems, the same doubling time for MDCK and pancreatic spheres, twice faster for epiblasts (Fig. 5b), and stronger adhesion force for MDCK cells (Ext. Fig. 3). We obtained phenotypes similar to MDCK cysts (Fig. 5b blue, see also Movie 9); for larger luminal pressure with the same proliferation time (green), fusion looked similar to pancreatic spheres (Movie 10); and for low luminal pressure and lower proliferation time, we could mimic qualitatively the behavior for epiblasts. Quantifications of lumen index in the numerical cysts for each case reproduced also the quantifications of experimental lumen index (compare Fig. 5d with Fig. 4c). However, the epiblast case lacked the transformation of the cyst shape. We therefore prepared numerical epiblasts similar to the experimental system with two lumens and small luminal pressure (Movie 11) with an elongated configuration similar to the experimental case (compare Fig. 4b and Fig. 5e). Based on experimental measurements in this configuration (Fig. 4i-k), we imposed radial cell motion (Fig. 5e) and we recapitulated successfully the fusion (Fig. 5f) as well as cell motion within the cyst (Fig. 5g,h) and axis ratio of the cyst (Fig. 5i). Finally, to further validate the relevance of our simulations to experimental data, we quantified the dynamics *in silico* of the three systems from initial stages by counting

177 the number of lumens as a function of time. Strikingly we could reproduce the biphasic behaviour for all
178 systems (Fig. 5c). These simulations support the importance of the interplay between cell proliferation,
179 cell adhesion and luminal growth in setting quantitatively lumen dynamics across systems.

180 Our modeling and experimental observations suggested that lumen growth, adhesion between cells and
181 cellular properties governed the differences between the three systems. We further tested this
182 experimentally using the MDCK system as a reference and perturbing these parameters. To evaluate the
183 role of lumen growth in fusion, we prepared MDCK cysts with two lumens and we designed an inflation
184 experiment using a micro-pipette to inject fluid[21] (Fig. 6a). To show the fusion, we used dextran in the
185 pipette. We could induce the fusion within minutes. This suggests that an increase in lumen growth rate
186 can drive fusion of MDCK lumen faster than it normally takes, along the result of a faster response
187 promoted by an increase of lumen volume in pancreatic spheres. The apparent role of cell-cell adhesion
188 for MDCK cysts was further tested by simultaneously decreasing cadherin-mediated adhesion by chelating
189 calcium with EDTA and using an anti E-cadherin blocking antibody[22,23] (Fig. 6b). We observed that lumen
190 number is significantly decreased, suggesting that lumen fusion was facilitated (Fig. 6b,c). This suggests
191 that adhesion between cells is an impediment to fusion in MDCK cysts. In addition, we tested the
192 behaviour of E-cadherin KO MDCK cell line for 8 cells and 16 cells initial conditions: the biphasic behaviour
193 was reproduced but this E-cadherin cell line presented a faster fusion (see Fig. 6d,e,f). This further
194 confirms that adhesion between cells can prevent fusion. Finally, to test the impact of cellular properties
195 on lumen formation, we used a MDCK cell line in which the tight junction proteins ZO1 and ZO2 were
196 knocked-out[21,24]. This cell line was shown to have smaller LI due to increased apical contractility[21] and
197 resembled the epiblast case with smaller lumen and elongated cells (see Extended Fig. 4a). We initiated
198 the MDCK ZO1/ZO2 KO cysts with 1 to 16 cells and we repeated the observation of the number of lumens
199 as a function of time and initial cell numbers (Fig. 6g,h). The results show that fusion was facilitated in the
200 ZO1/ZO2 KO cyst. Several features of this ZO1/ZO2 mutant MDCK cyst corresponded with epiblasts cysts,
201 such as low LI and similar mechanical response to inflation (Extended Fig. 4), as well as facilitated fusion
202 as a function of cell number. This suggests that tight junction deletion contributes to faster fusion. These
203 experiments of MDCK cysts transformations with mechanical or biological perturbations support the
204 notion that lumen fusion generically results from this interplay between luminal pressure and mechanical
205 cell interactions.

206 **Discussion.**

207 We have shown that the number of lumens depends on the initial cell number and their evolution exhibits
208 similar biphasic behaviours for MDCK, pancreatic spheres and epiblasts (Fig. 7). The nucleation phase is
209 dictated mainly by appearance of new lumens whereas the second phase is dominated by fusion to reach
210 a single lumen for all systems. Nucleation mechanisms are shared between MDCK cells and pancreatic
211 spheres both when cells divide and when two cells adhere to each other, whereas epiblasts need about
212 10 cells to nucleate a lumen. MDCK and pancreatic spheres fusions are predominantly driven by an
213 increase in lumen index, whereas fusion is determined by cell motion in epiblasts with low lumen index.
214 Our experimental perturbations of MDCK fusions suggest that luminal pressure in competition with cell-
215 cell adhesion controls fusion. In pancreatic spheres the lumen index is larger than the MDCK cysts and
216 fusion is likely driven by luminal ion pumping, whereas epiblasts fusions are dominated by cells motion.

217 The mechanism of lumen nucleation after cell division was reported in MDCK [6,25,26]. It is consistent with
218 the nucleation mechanism we report for MDCK and we report it for pancreatic spheres. In addition, we

also add the lumen nucleation associated to contact between cells as well, which supports the notion that several mechanisms of lumen nucleation could co-exist with similar timing. It is worth noting that lumen nucleation was reported in an assay between cadherin coated surface and a single cell[27] which suggests that adherens junctions formation between cells *per se* could trigger lumen formation. Finally, we report the larger number of cells needed to nucleate a lumen for epiblasts and it is consistent with Ref. 28,29. Despite these multiple mechanisms for lumen nucleation, we report and explain in a unified way the mechanisms for the nucleation phase I across systems.

We distinguish fusion between lumens triggered by ion-pumping mechanisms leading to an effective increase in hydrostatic pressure of the lumen in competition with cell-cell adhesion and fusion between lumens triggered by cell re-organisation. This difference can be understood by a simple force balance argument: when the lumen index is large, the hydrostatic pressure of the lumen pushes the cell apical side and the cell monolayer thereby competing with cell-cell contacts; in contrast, when lumen index is low, the hydrostatic pressure of the lumen is low and interactions between cells essentially determine the potential fusion between lumens. Lumen fusion by increased osmotic pressure was reported in various situations *in vitro* and *in vivo*[12,30,31] along our observations and this illustrates that common rules of self-organisation across systems could determine the morphogenesis of organs in 3D.

We propose that these generic nucleation and fusion mechanisms could be tested on other organoid systems. The timing of cell proliferation compared to lumen fusion dynamics could be tuned to optimize the target size of the organ with the relevant cell number and the number and size of lumens. Systems may select fast pumping like the pancreas to allow multiple lumens to fuse rapidly with potential change in luminal pressure to form a single duct[32]. In contrast, systems which would need to keep compartments such as the thyroid gland may have developed larger adhesion properties to prevent fusion and allow each zone to keep potential differences in composition[33].

Along this hypothesis, it is interesting to note that cells change their states in the case of epiblasts[34]. From stem cells, they exit from pluripotency and follow paths of differentiation leading to the right localization in the final organs. We propose that this orchestration of proliferation with lumens nucleation and fusion could also be optimized to generate organs with the relevant shape and cell numbers but also with the right cell state distributions. Future experiments coupling our approach with spatial transcriptomics will allow to test this hypothesis.

Our results could shed light on the synthesis of artificial organs. Indeed, it was reported that cell printing was a promising method to generate organs[35,36]. Our results show that the cell number at plating, their growth rates, and their fusions, contribute to the dynamics of the organs formation. This initial condition correlates with morphology and functions of organ. As a result, a due care to the force balance would need to be evaluated in the synthesis of organs and our framework with its numerical simulations could serve as a solid basis to predict the future shape of the targeted organs.

Acknowledgements.

We thank the Riveline group for help and discussions and Erwan Grandgirard and the Imaging Platform of IGBMC. We also thank Byung Ho Lee and Allison Lewis for experimental, conceptual and image analysis advice and discussions. We thank Benoît Ladoux for providing the MDCKII E- cadherin KO cell line. L.L. and

T.G. are supported by HFSP and by the University of Strasbourg and by la Fondation pour la Recherche Médicale. D.R. acknowledges the Interdisciplinary Thematic Institute IMCBio, part of the ITI 2021-2028 program of the University of Strasbourg, CNRS and Inserm, which was supported by IdEx Unistra (ANR-10-IDEX-0002), and by SFRI-STRAT'US project (ANR 20-SFRI-0012) and EUR IMCBio (ANR-17-EURE-0023) under the framework of the French Investments for the Future Program. A.G.B, A.H., M.S. and D.R. acknowledge the Research Grant from Human Frontier Science Program (Ref.-No: RGP0050/2018).

Materials and Methods.

Cell sources and expansion

We used 3 cellular systems, MDCK II cell lines, mouse embryonic cells (mES cells)[37], and pancreatic spheres[38]. Other mutant cell lines were used for MDCK: MDCK II E-cadherin-GFP/Podocalyxin-mScarlett/Halo-CAAX[39], MDCK II ZO1/2-KO[21] and MDCK II E-cadherin KO[40].

The MDCK II cell lines were cultured in MEM (Gibco 410900028) with 5 % Fetal Bovine Serum (Sigma, USA), 1mM Sodium Pyruvate (Gibco 11360-070) and 1x NEAA (Gibco 11140050). MDCKII cells were resuspended every 2 to 3 days with trypsin-EDTA after they reached 70-95% confluency. A seeding density of about $3*10^5$ cells per 75 cm^2 was used for sub-culture. R1 ES-cell line was used for the culture of epiblast. Mouse embryonic stem cells were expanded with 1:1 DMEM/F12 (ThermoFischer 31331028) and neurobasal medium (Gibco 21103049) supplemented with 1x N2 (Gibco 17502048), 1x B27 (Gibco 12587010) and 1x NEAA (Gibco 11140050), 55µM 2-Mercaptoethanol (Gibco 21985023), 3µM CHIR 99021 (Sigma SML 1046-5mg) and 2x LIF produced at IGBMC-Strasbourg in non-adhesive flasks[37]. Cells were sub-cultured every 4 days until the size of spheres reached a diameter of 80µm. Pancreatic spheres were prepared from the dissection of E13.5 embryos (mouse CD1 from Charles River Laboratory) using the protocol reported in Greggio et al[38] and used without passaging.

Cells diameter measurement.

For the three systems, single cells were plated after trypsinisation and labeled using 10nM SiR-actin (TEBU-BIO, 251SC001). The middle planes of spherical cells were imaged. The associated surfaces were measured with Fiji and the distributions of cells diameters were plotted (see Ext. Fig. 1). Cavities diameters were designed accordingly by taking the mean value of each distribution to control the initial cell numbers (Ext. Fig. 1c). All cavities had a cell height from 10µm to 17µm to keep the height similar to one cell diameter.

Microfabrication and cavity map.

We designed the samples with a map of patterns for cavities in order to: (i) track the evolution of the same cysts up to a week, (ii) test a large number of cysts with the same initial cell number and (iii) test the effects of different initial cell numbers for the same biological repeat (see Fig. 1a). The same strategy was adapted for each system by designing the cavity map accordingly.

Cavities were prepared using soft lithography as described in Bhat et al[16]. Briefly, we designed a mask with AutoCad to obtain a large number of motifs and different diameters. The motifs were selected to contain many initial cells number conditions. We used the following calculation of the motif's diameter, rescaled

297 with the mean cell diameter: S(surface of cavities)= number of initial cells*surface of cells. These designs
298 were printed on photomask and then we transfer these patterns on SU-8 silicon wafer with soft
299 lithography. Next the design was replicated on a PDMS mold. Finally, these designs were transferred to
300 cover-glass which allows us to achieve higher resolution images.

301 **Cell seeding in microfabricated cavities for the control of initial cell number.**

302 To generate cysts and organoids in micro-fabricated cavities, we seeded cells in micro-cavities with the
303 following steps based on our former protocol[16,41]. Briefly, (i) the microfabricated-cavities on coverslips
304 were activated with O_2 plasma (Diener); (ii) substrates were incubated with 5µg/ml laminin (Sigma
305 11243217001) for 1 hour at room temperature followed by washing steps; (iii) cells in suspension were
306 centrifuged 3 times at 1000 rpm for 3 minutes on the samples to direct cells inside micro-cavities; (iv) the
307 coverslips were then rinsed gently to get rid of the excess of cells between cavities; (v) 15 µl Matrigel
308 (Corning, 356231) was added on top of the sample. After solidification of the Matrigel, the relevant media
309 were added depending on the cyst types. For pancreas spheres, single cells were dissociated from the
310 E13.5 pancreases and immediately seeded in the micro-well without centrifugation.

311 System-specific media were added to obtain pancreatic spheres or epiblasts. Pancreatic sphere was
312 formed by using DMEM/F12 (ThermoFischer 31331028) with B27 (Gibco 17504-044), recombinant Human
313 FGF2 (R&D 233-FB-025), Y-27632 (Sigma Aldrich ab120129) and Penicillin-Streptomycin (Gibco 15070-
314 063)[38]. Epiblasts were differentiated by using 1:1 ratio of DMEM/F12 (ThermoFischer 31331028) and
315 neurobasal medium (Gibco 21103049) containing 0.5x N2 (Gibco 17502048), 1x B27 with vitamin A (Gibco
316 12587010), 1x NEAA (Gibco17504044), 0.1mM 2-Mercaptoethanol (Gibco 21985023), 0.15mM Sodium
317 Pyruvate and 0.2mM LGlutamaine (Life Technology GmbH 11360039).

318 **Immunostaining.**

319 For immunostaining, we followed standard protocols Greggio, C. et al[42]. Briefly, samples were washed
320 with PBS and fixed with 4% paraformaldehyde (Electron Microscopy Sciences 15710) diluted in PBS for 15
321 minutes. Cells were permeabilized with 0.5% Triton-X-100 for 15 minutes and then a blocking solution
322 made of 1% Normal Goat Serum in PBS 1X was added overnight. Primary antibodies were added directly
323 to the blocking solution for two days at 4°C. Following 3 successive washing steps with PBS, the samples
324 were stained with the relevant secondary antibodies for 2 hours at room temperature. We used the
325 following primary antibodies: Anti-E-cadherin (Abcam, Ab11512 and Ab53033), Mouse monoclonal Anti-
326 Podocalyxin (BIO-TECHNE SAS, MAB1556-SP), Alexa Fluor Phalloidin 488 (ThermoFisher, A12379) for F-
327 actin and DAPI (Sigma MBD0015) for the nucleus. Samples were washed three times in PBS and mounted
328 on a home-made sample holder system for imaging and conservation.

329 **Microscopy.**

330 In order to track the number of lumens in MDCK cysts, MDCK cells expressing Ecad – Podxl were used to
331 visualize adherens junctions and apical side, respectively. After cell seeding, images were taken at an
332 interval of 24 hours using Leica DMI8 with an Evolve 512 camera coupled to a spinning disk microscope
333 (CSU W1) with a 25x water objective (NA = 0.9) and 63x glycerol objective (NA = 1.2) using the software
334 Metamorph for image acquisition. Positions were chosen based on initial cell numbers and the same
335 MDCKII cysts were acquired in 3D every 24h. This was possible with the cavity map reported above. For

336 pancreatic spheres and epiblasts, initial conditions were controlled with the same method and samples
337 were fixed and stained with the relevant antibodies before 3D acquisition with the same microscopy
338 setup.

339 To record the lumen formation in MDCK, MDCK cysts were imaged at a time interval of 5 min for more
340 than 24 hours in a setup regulated for 5% CO_2 and 37°C temperature. We used MDCK cells stably
341 expressing E-cadherin-GFP and podocalyxin as readouts for cells junction and lumen. To record the lumen
342 nucleation in pancreatic spheres, we imaged them live after cells seeding with phase contrast microscopy
343 (Fig. 3d). For the characterisation of lumen nucleation in epiblasts, we fixed samples with every 8 hours
344 after cells seeding and we stained for E-cadherin and podocalyxin prior imaging (Fig. 3f).

345 For lumen fusion events in MDCK cysts, we used a 63x glycerol objective (N.A.= 1.2). Different organoids
346 were selected as starting positions and imaged every 30 min for up to 3 days. Z-stacks (60 µm range, 1 µm
347 step) were acquired. For lumen fusion in epiblasts, epiblasts were imaged from day 2 with SiR-actin (TEBU-
348 BIO, 251SC001) after 1 hour incubation before the experiment. Then SiR-actin mix were incubated with
349 media leading to a final concentration of SiR-actin and Verapamil. The concentrations were larger for
350 MDCK cysts for optimal visualisation. Lumen interaction events were recorded with a Leica CSU-W1
351 spinning disk (63× objective) for more than 10 hours at an interval time of 30 min.

352 **Perturbation experiments.**

353 For the inflation experiment[21] (Fig. 6a), MDCK cysts were used after 5 days of culture. We first removed
354 gently Matrigel from the top of micro-wells with a needle. The lumen was inflated by flowing media
355 containing fluorescent dextran (Fisher Scientific SAS D22914) in the relevant media with a micro-pipette
356 and images were taken using Leica spinning disk equipped with micromanipulators. To investigate the role
357 of adhesion in lumen fusion, we used 5 mM EDTA and E-cadherin 10 µg/ml antibody[22,23] (Fig. 6b).
358 Snapshots of MDCK cells were taken right before addition of EDTA/E-cadherin antibody and then the cysts
359 were acquired in 3D for 60 minutes to record the fusion events.

360 **Imaging and data analysis.**

361 To extract the shapes and measure the volumes and surfaces of lumens and organoids, we used LimeSeg
362 Fiji Plugin and Skeleton Seg. The segmented 3D structures were saved and visualized. Analysis and
363 quantification were performed with Paraviewer[43].

364 The number of lumens were rescaled with respect to the cell cycle (Fig. 3a and Fig. 4a) by dividing the
365 number of lumens by the duration of each cell cycle. We evaluate 18h for MDCK, 18h for pancreatic
366 spheres, and 9h for epiblasts. We checked that doubling times were consistent with the number of cells
367 counted in each system. In addition, we define lumen as a fluid-filled cavity between cells within the
368 optical resolution together with accumulation of apical marker such as podocalyxin and F-actin. Lumen
369 index is defined as the ratio between the area of lumen and the area of the outer shell of the cyst. They
370 were measured for each system. The numerical lumen index was measured by taking 2D lumen surface
371 over cyst surface. To compare the fusion process between MDCK cyst and epiblast, we ellipse fitted the
372 outer contour of cysts to extract the long and short axis. Then, we plotted the major axis over the minor

axis as a function of time (Figure 4f,i). To characterize the associated cell motion during fusion, we plotted cell trajectories by using tracking their centers (Figure 4h,k).

Data were plotted using a written Python code and GraphPad Prism. Statistical tests were performed using non-parametric Mann-Whitney test (two-tailed) to evaluate the significance between lumen formation after cell division and when cells met (Figure 3c,e), lumen occupancy (Ext. Fig. 3b), intensity of E-cadherin (Ext. Fig 3c), and the difference of number of lumens between WT MDCK cyst and ZO-KO cyst (Figure 6h). The differences of number of lumens before and after EDTA+ anti-E-cadherin treatment were assessed for statistical significance by using Wilcoxon matched-pairs signed rank test (Figure 6c). Differences between groups for the pipette inflation experiment were analysed for statistical significance by ANOVA. Statistical significance was indicated using the following symbols: ns p-value >0.05, * $p < 0.05$, ** $p < 0.01$ and *** $p < 0.001$.

The number of experimental repeats and number of cyst or organoids are indicated in the Figure captions.

Theoretical model and numerical simulations.

The cyst was theoretically modeled based on the multi-cellular phase field model with lumen[19] but additionally incorporating the extracellular matrix around the cyst. To carefully control the surface tension of each entity (each cell, lumen, ECM), we applied the resharpening method proposed in Refs. 44,45, which enabled us to eliminate the surface tension artificially generated due to the construction principle of the phase field model. The details of this theoretical model are given in Supplementary Note Theory.

Materials, Data and Code availability.

All materials will be available upon reasonable request.

The Data are available upon request and the software Code used for the simulation is available in the Github, https://github.com/kana-fuji/MCPFM_for_Lumen_Fusion.git

----

Movies Captions.

Movie 1 - Lumen nucleation after cell division for MDCK cyst. MDCK cells expressing E-cadherin in green and Podocalyxin. Time in hh:mm:ss.

Movie 2 - Lumen nucleation after cells meet for MDCK cyst. MDCK cells expressing E-cadherin in green and Podocalyxin. Time in hh:mm:ss.

Movie 3 - Lumen nucleation after cell division for pancreatic sphere. Time in hh:mm.

Movie 4 - Lumen nucleation after cells meet for pancreatic sphere. Time in hh:mm.

Movie 5 - Lumen increase in volume leads to lumen fusion for MDCK cyst. MDCK cells expressing E-cadherin in green and Podocalyxin in red with 8 cells as initial conditions. Time in hh:mm.

Movie 6 - Lumen increase in volume leads to lumen fusion for pancreatic spheres. Pancreatic spheres were imaged with 8 cells as initial condition. Time in hh:mm.

407 **Movie 7 -** Centripetal motion with low lumen occupancy leads to lumen fusion in epiblast. Time in hh:mm.

408 **Movie 8 -** Simulation movie of typical numerical evolution of cysts.

409 **Movie 9 -** Simulation movie of lumen interaction and fusion for 8 cells condition – with a dynamic similar
410 to MDCK cyst.

411 **Movie 10 -** Simulation movie of lumen interaction and fusion for 8 cells – with a dynamic similar to
412 pancreatic sphere.

413 **Movie 11 -** Simulation movie of lumen fusion for 8 cells condition – with a dynamic similar to epiblast.

414

415 **References.**

416

417 1. Zhu, M. & Zernicka-Goetz, M. Principles of Self-Organization of the Mammalian Embryo. *Cell* **183**,
418 1467–1478 (2020).
419 2. Wennekamp, S., Mesecke, S., Nédélec, F. & Hiiragi, T. A self-organization framework for symmetry
420 breaking in the mammalian embryo. *Nat Rev Mol Cell Biol* **14**, 452–459 (2013).
421 3. Hannezo, E. & Simons, B. D. Multiscale dynamics of branching morphogenesis. *Current Opinion in Cell*
422 *Biology* **60**, 99–105 (2019).
423 4. Martín-Belmonte, F. *et al.* Cell-Polarity Dynamics Controls the Mechanism of Lumen Formation in
424 Epithelial Morphogenesis. *Current Biology* **18**, 507–513 (2008).
425 5. Strilić, B. *et al.* The Molecular Basis of Vascular Lumen Formation in the Developing Mouse Aorta.
426 *Developmental Cell* **17**, 505–515 (2009).
427 6. Mangan, A. J. *et al.* Cingulin and actin mediate midbody-dependent apical lumen formation during
428 polarization of epithelial cells. *Nat Commun* **7**, 12426 (2016).
429 7. Sigurbjörnsdóttir, S., Mathew, R. & Leptin, M. Molecular mechanisms of de novo lumen formation.
430 *Nat Rev Mol Cell Biol* **15**, 665–676 (2014).
431 8. Datta, A., Bryant, D. M. & Mostov, K. E. Molecular regulation of lumen morphogenesis. *Curr Biol* **21**,
432 R126-136 (2011).

433 9. Mailleux, A. A., Overholtzer, M. & Brugge, J. S. Lumen formation during mammary epithelial
434 morphogenesis: insights from in vitro and in vivo models. *Cell Cycle* **7**, 57–62 (2008).
435 10. Dasgupta, S., Gupta, K., Zhang, Y., Viasnoff, V. & Prost, J. Physics of lumen growth. *Proc Natl*
436 *Acad Sci U S A* **115**, E4751–E4757 (2018).
437 11. Torres-Sánchez, A., Kerr Winter, M. & Salbreux, G. Tissue hydraulics: Physics of lumen formation
438 and interaction. *Cells & Development* **168**, 203724 (2021).
439 12. Dumortier, J. G. *et al.* Hydraulic fracturing and active coarsening position the lumen of the
440 mouse blastocyst. *Science* **365**, 465–468 (2019).
441 13. Li, Q. *et al.* Extracellular matrix scaffolding guides lumen elongation by inducing anisotropic
442 intercellular mechanical tension. *Nat Cell Biol* **18**, 311–318 (2016).
443 14. Sato, T. *et al.* Single Lgr5 stem cells build crypt-villus structures in vitro without a mesenchymal
444 niche. *Nature* **459**, 262–265 (2009).
445 15. Yang, Q. *et al.* Cell fate coordinates mechano-osmotic forces in intestinal crypt formation. *Nat*
446 *Cell Biol* **23**, 733–744 (2021).
447 16. Bhat, A. *et al.* How to orient cells in microcavities for high resolution imaging of cytokinesis and
448 lumen formation. in *Methods in Cell Biology* vol. 158 25–41 (Elsevier, 2020).
449 17. Taniguchi, K. *et al.* Lumen Formation Is an Intrinsic Property of Isolated Human Pluripotent Stem
450 Cells. *Stem Cell Reports* **5**, 954–962 (2015).
451 18. Nonomura, M. Study on Multicellular Systems Using a Phase Field Model. *PLoS ONE* **7**, e33501
452 (2012).
453 19. Akiyama, M., Nonomura, M., Tero, A. & Kobayashi, R. Numerical study on spindle positioning
454 using phase field method. *Phys. Biol.* **16**, 016005 (2018).

455 20. Tanida, S. *et al. The interplay between lumen pressure and cell proliferation determines organoid*
456 *morphology in a multicellular phase field model*.
457 http://biorxiv.org/lookup/doi/10.1101/2023.08.17.553655 (2023) doi:10.1101/2023.08.17.553655.
458 21. Mukenhirn, M. *et al. Tight junctions regulate lumen morphology via hydrostatic pressure and*
459 *junctional tension*. http://biorxiv.org/lookup/doi/10.1101/2023.05.23.541893 (2023)
460 doi:10.1101/2023.05.23.541893.
461 22. Harris, A. R., Daeden, A. & Charras, G. T. Formation of adherens junctions leads to the
462 emergence of a tissue-level tension in epithelial monolayers. *Journal of Cell Science* jcs.142349 (2014)
463 doi:10.1242/jcs.142349.
464 23. Comelles, J. *et al.* Epithelial colonies in vitro elongate through collective effects. *eLife* **10**, e57730
465 (2021).
466 24. Otani, T. *et al.* Claudins and JAM-A coordinately regulate tight junction formation and epithelial
467 polarity. *Journal of Cell Biology* **218**, 3372–3396 (2019).
468 25. Li, D., Mangan, A., Cicchini, L., Margolis, B. & Prekeris, R. FIP 5 phosphorylation during mitosis
469 regulates apical trafficking and lumenogenesis. *EMBO Rep* **15**, 428–437 (2014).
470 26. Zieger, E. *et al.* Midbody-Localized Aquaporin Mediates Intercellular Lumen Expansion During
471 Early Cleavage of an Invasive Freshwater Bivalve. *Front. Cell Dev. Biol.* **10**, 894434 (2022).
472 27. Zhang, Y. *et al.* Biomimetic niches reveal the minimal cues to trigger apical lumen formation in
473 single hepatocytes. *Nat. Mater.* **19**, 1026–1035 (2020).
474 28. Shahbazi, M. N. *et al.* Pluripotent state transitions coordinate morphogenesis in mouse and
475 human embryos. *Nature* **552**, 239–243 (2017).
476 29. Kim, Y. S. *et al.* Deciphering epiblast lumenogenesis reveals proamniotic cavity control of
477 embryo growth and patterning. *Sci. Adv.* **7**, eabe1640 (2021).

478 30. Alvers, A. L., Ryan, S., Scherz, P. J., Huisken, J. & Bagnat, M. Single continuous lumen formation
479 in the zebrafish gut is mediated by *smoothened* -dependent tissue remodeling. *Development* **141**,
480 1110–1119 (2014).
481 31. Bagnat, M., Cheung, I. D., Mostov, K. E. & Stainier, D. Y. R. Genetic control of single lumen
482 formation in the zebrafish gut. *Nat Cell Biol* **9**, 954–960 (2007).
483 32. Dahl-Jensen, S. B. *et al.* Deconstructing the principles of ductal network formation in the
484 pancreas. *PLoS Biol* **16**, e2002842 (2018).
485 33. Gonay, L. *et al.* Modelling of Epithelial Growth, Fission and Lumen Formation During Embryonic
486 Thyroid Development: A Combination of Computational and Experimental Approaches. *Front.*
487 *Endocrinol.* **12**, 655862 (2021).
488 34. Bedzhov, I. & Zernicka-Goetz, M. Self-Organizing Properties of Mouse Pluripotent Cells Initiate
489 Morphogenesis upon Implantation. *Cell* **156**, 1032–1044 (2014).
490 35. Noor, N. *et al.* 3D Printing of Personalized Thick and Perfusable Cardiac Patches and Hearts.
491 *Advanced Science* **6**, 1900344 (2019).
492 36. Jorgensen, A. M. *et al.* Multicellular bioprinted skin facilitates human-like skin architecture in
493 vivo. *Sci. Transl. Med.* **15**, eadf7547 (2023).
494 37. Martin-Lemaitre, C., Alcheikh, Y., Naumann, R. & Honigmann, A. *Optimization of mouse*
495 *embryonic stem cell culture for organoid and chimeric mice production*.
496 http://biorxiv.org/lookup/doi/10.1101/2020.03.13.990135 (2020) doi:10.1101/2020.03.13.990135.
497 38. Greggio, C., De Franceschi, F., Figueiredo-Larsen, M. & Grapin-Botton, A. In Vitro Pancreas
498 Organogenesis from Dispersed Mouse Embryonic Progenitors. *JoVE* 51725 (2014) doi:10.3791/51725.
499 39. Lu, L. *et al. Polarity-driven three-dimensional spontaneous rotation of a cell doublet*.
500 http://biorxiv.org/lookup/doi/10.1101/2022.12.21.521355 (2022) doi:10.1101/2022.12.21.521355.

40. Balasubramaniam, L. *et al.* Investigating the nature of active forces in tissues reveals how contractile cells can form extensile monolayers. *Nat. Mater.* **20**, 1156–1166 (2021).

41. Wollrab, V., Thiagarajan, R., Wald, A., Kruse, K. & Riveline, D. Still and rotating myosin clusters determine cytokinetic ring constriction. *Nat Commun* **7**, 11860 (2016).

42. Greggio, C. *et al.* Artificial three-dimensional niches deconstruct pancreas development *in vitro*. *Development* **140**, 4452–4462 (2013).

43. Ahrens, J., Geveci, B. & Law, C. ParaView: An End-User Tool for Large-Data Visualization. in *Visualization Handbook* 717–731 (Elsevier, 2005). doi:10.1016/B978-012387582-2/50038-1.

44. Olsson, E. & Kreiss, G. A conservative level set method for two phase flow. *Journal of Computational Physics* **210**, 225–246 (2005).

45. Badillo, A. Quantitative phase-field modeling for boiling phenomena. *Phys. Rev. E* **86**, 041603 (2012).

Figure 1

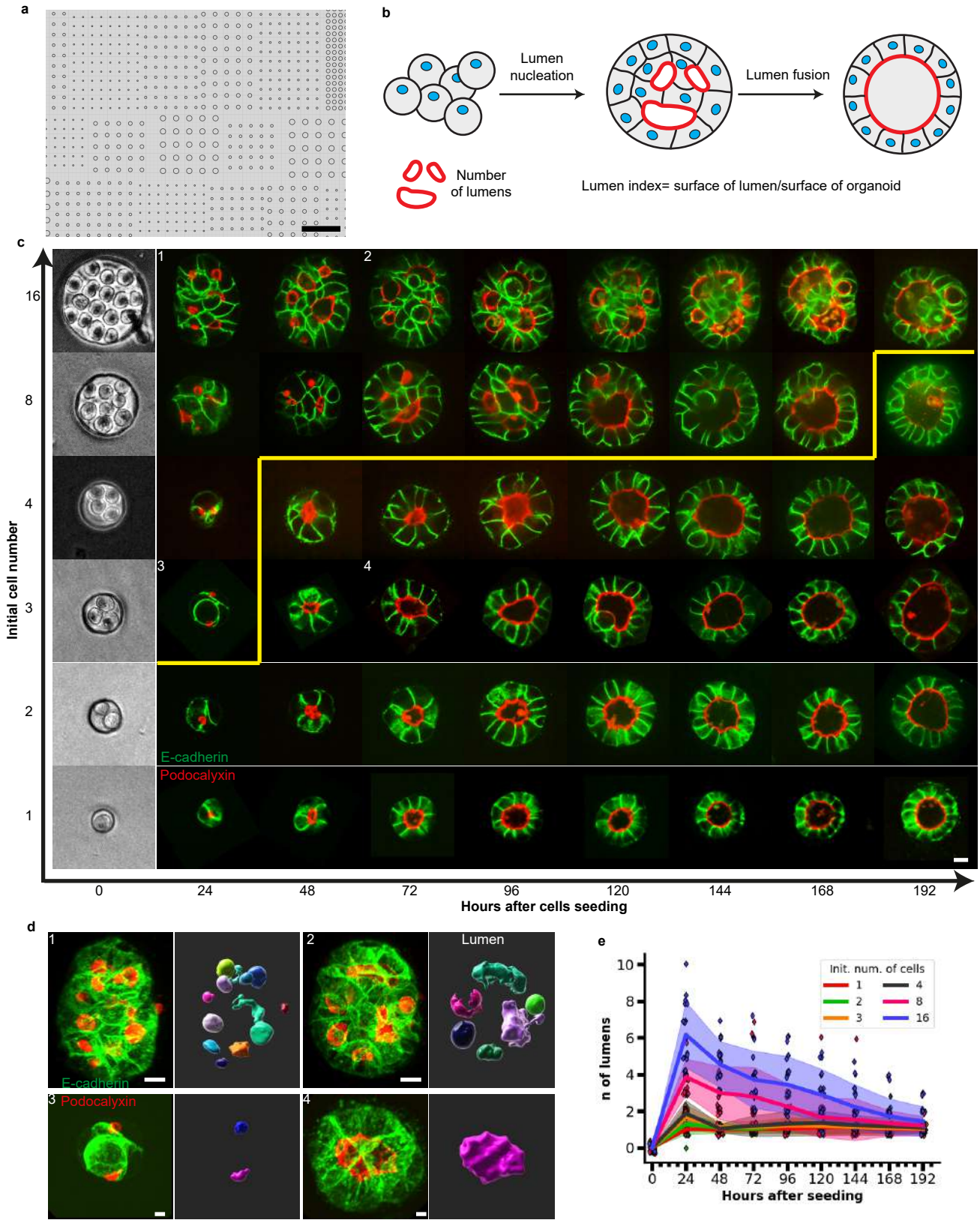

Figure 1 - Lumen nucleation and fusion in MDCK spheres with controlled initial cell numbers. a. Mask for the design of the cavity map. Cavities of different diameters were arrayed and designed to accommodate different initial cell numbers. Scale bar 200µm. b. Schematic representation of lumenogenesis. Dissociated plated cells adhere to each other and then lumens (surrounded by red line) are nucleated and eventually fuse. c. Typical dynamics of MDCK cysts forming from controlled initial cell numbers (E-cadherin in green, Podocalyxin in red). Initial cell numbers are shown at time 0 in cavities and the shapes of the same spheres are captured every day. The yellow line outlines the zone of MDCK cysts which reached the single lumen stage. Scale bar 10µm (N=3, n≥10). d. 3D visualization of four lumens and spheres corresponding to c and indicated as 1,2,3,4. left: 3D viewer of spheres with E-cadherin in green and Podocalyxin in red. Right: 3D viewer of lumen by Imaris, scale bar 10µm. e. Quantification of the number of lumens in MDCK spheres as a function of time for different initial cell number: 1,2,3,4,8,16 cells. The number of lumens increases over time and with initial cell number (see also Ext. Fig. 2). All cysts end up close to single lumens.

Figure 2

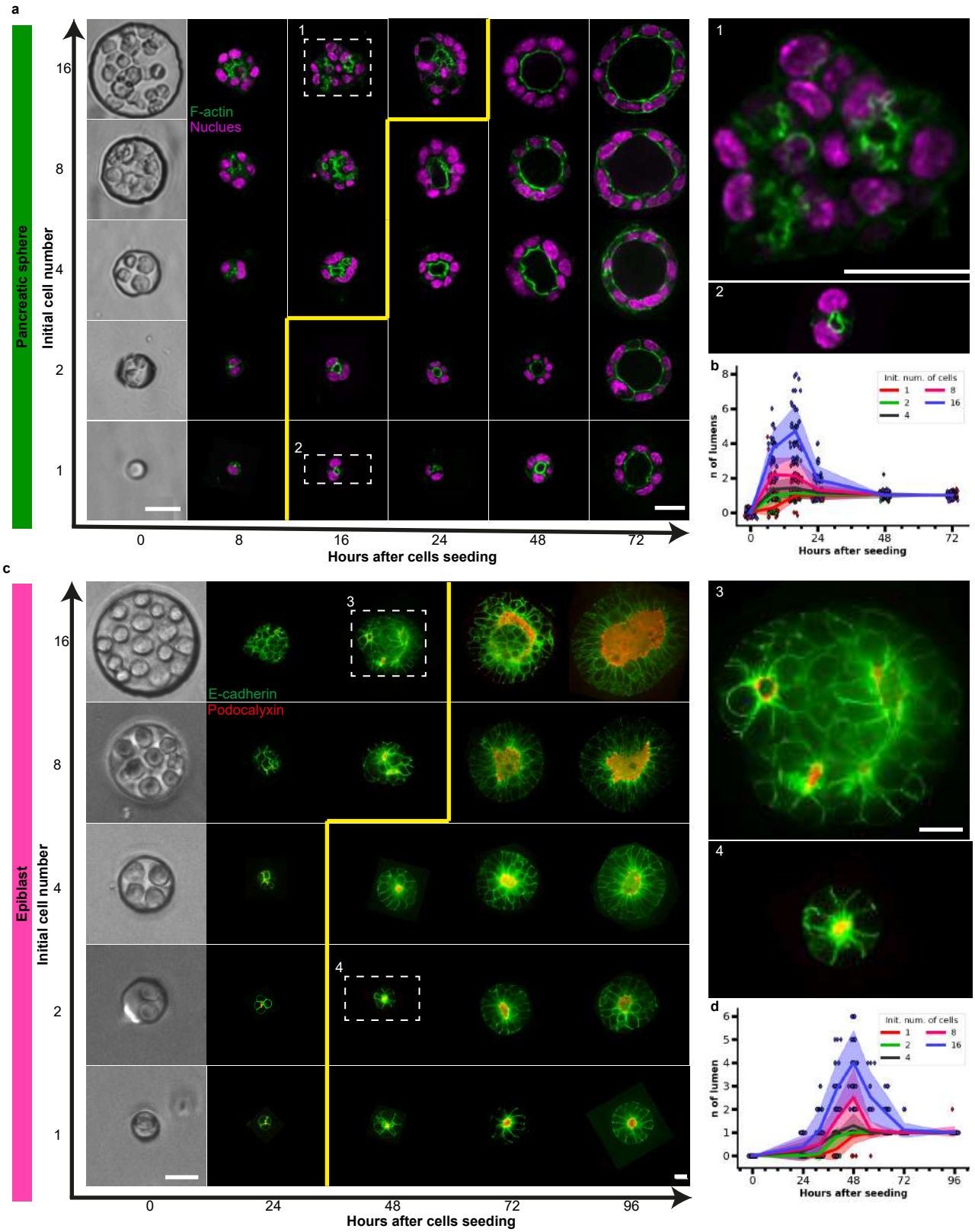

Figure 2 - Lumen nucleation and fusion in pancreatic and in epiblast spheres. a. Typical evolution of pancreatic spheres shapes as a function of initial cell number and time (F-actin in green, nucleus in Magenta) (N=3, n>20). Scale bars 10 µm at time 0 and at time 96 h with 3D zooms on outlined pancreatic spheres. b. Quantification of the number of lumens in pancreatic spheres as a function of time for different initial cell numbers: 1,2,4,8,16 cells. c. Typical evolution of epiblasts as a function of initial cell number and time (E-cadherin in green, Podocalyxin in red) (N=3, n>20). Scale bars 10 µm at time 0 and at time 72 h with 3D zooms on outlined epiblasts. d. Quantification of the number of lumens in epiblast as a function of time with different initial cell numbers, 1,2,4,8,16 cells. For a and c, the yellow line outlines the zone with single lumens. For both systems, the number of lumens increases as a function of time and with initial cell numbers. All cysts end up close to single lumens. Note that the timescales are different for the 3 systems indicated with the same colour code across the article (compare Fig. 2b, Fig. 2d and Fig. 1e).

Figure 3

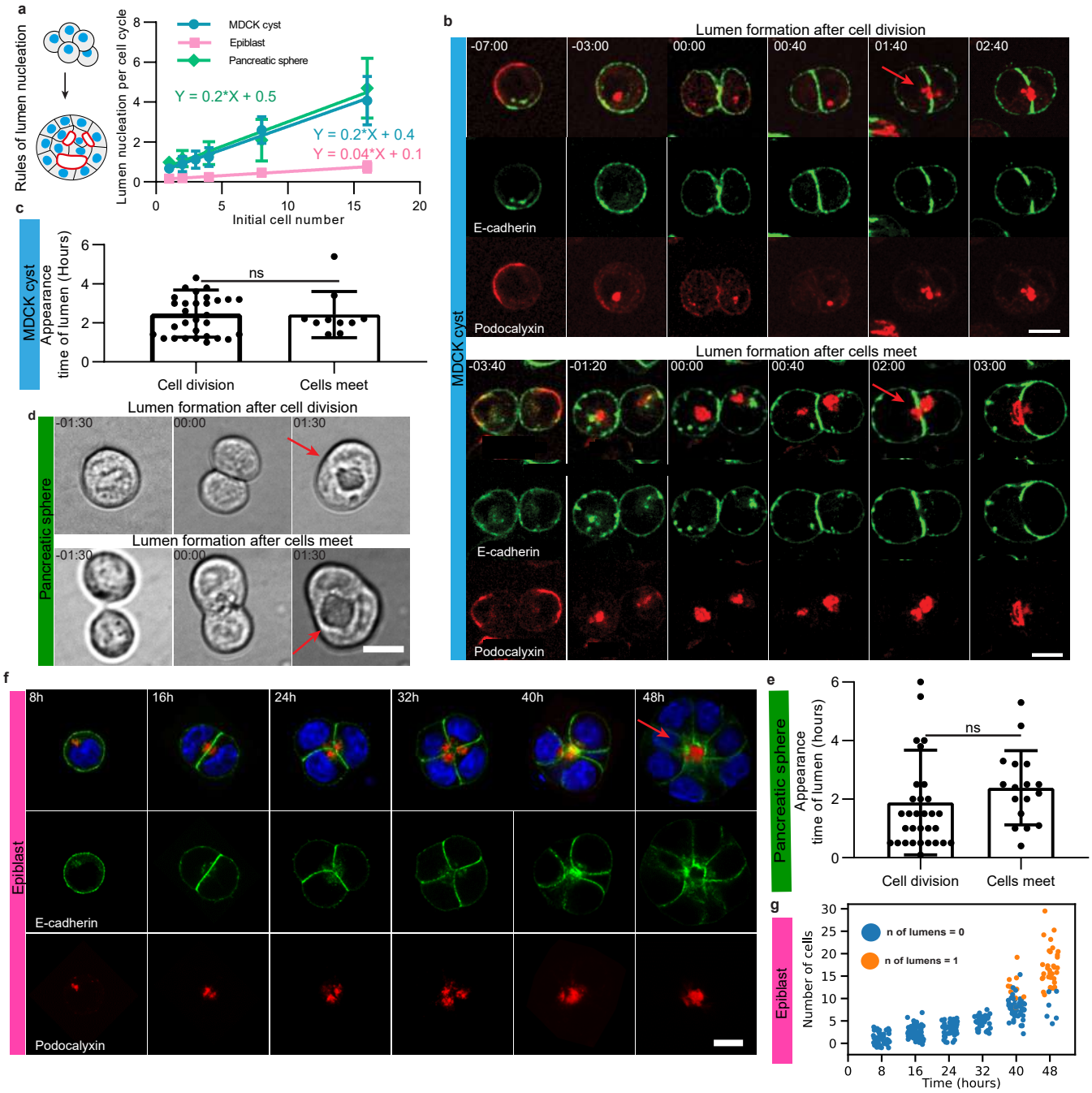

Figure 3 - Rules of lumen nucleation in the 3 systems. The lumens are nucleated after cell division and after cells meet in MDCK spheres and pancreatic spheres but they form after about 5 cell divisions in epiblasts. a. Lumen nucleation per cell cycle as a function of initial cell numbers, see Materials and Methods. The increase is linear for the 3 systems. MDCK and pancreatic spheres have the same slope whereas epiblasts have a slope 5 times lower. b. Snapshots of lumen nucleation in MDCK cysts. Top : Lumen formation after cell division in MDCK cysts (Movie 1) N=5, n=32. Bottom : Lumen formation after contacts between cells in MDCK cysts (Movie 2) N=4, n=10 (E-cadherin in green and Podocalyxin in red). Time relative to the junction formation set as time 0. Time in hh:mm. Scale bar 10 µm. c. Quantification of lumen appearance time after cell division or after cells meet. d. Snapshots of lumen nucleation in pancreatic spheres, Top: lumen formation after cell division, see also Movie 3. Bottom: lumen formation after two cells meet, see also Movie 4. Time relative to the junction formation set as time 0. Time in hh:mm. Scale bar 10 µm. The red arrows indicate lumen. e. Quantification of the lumen nucleation after cell division or after cells meet. f. Lumen nucleation in epiblasts fixed at 8h, 16h, 24h, 32h, 40h and 48h after cell seeding, stained with DAPI in blue, podoxalyxin in red and E-cadherin in green. g. Number of cells as a function of time with lumen appearance (N=2, n>10). ns indicates non-significant P value >0.05.

Figure 4

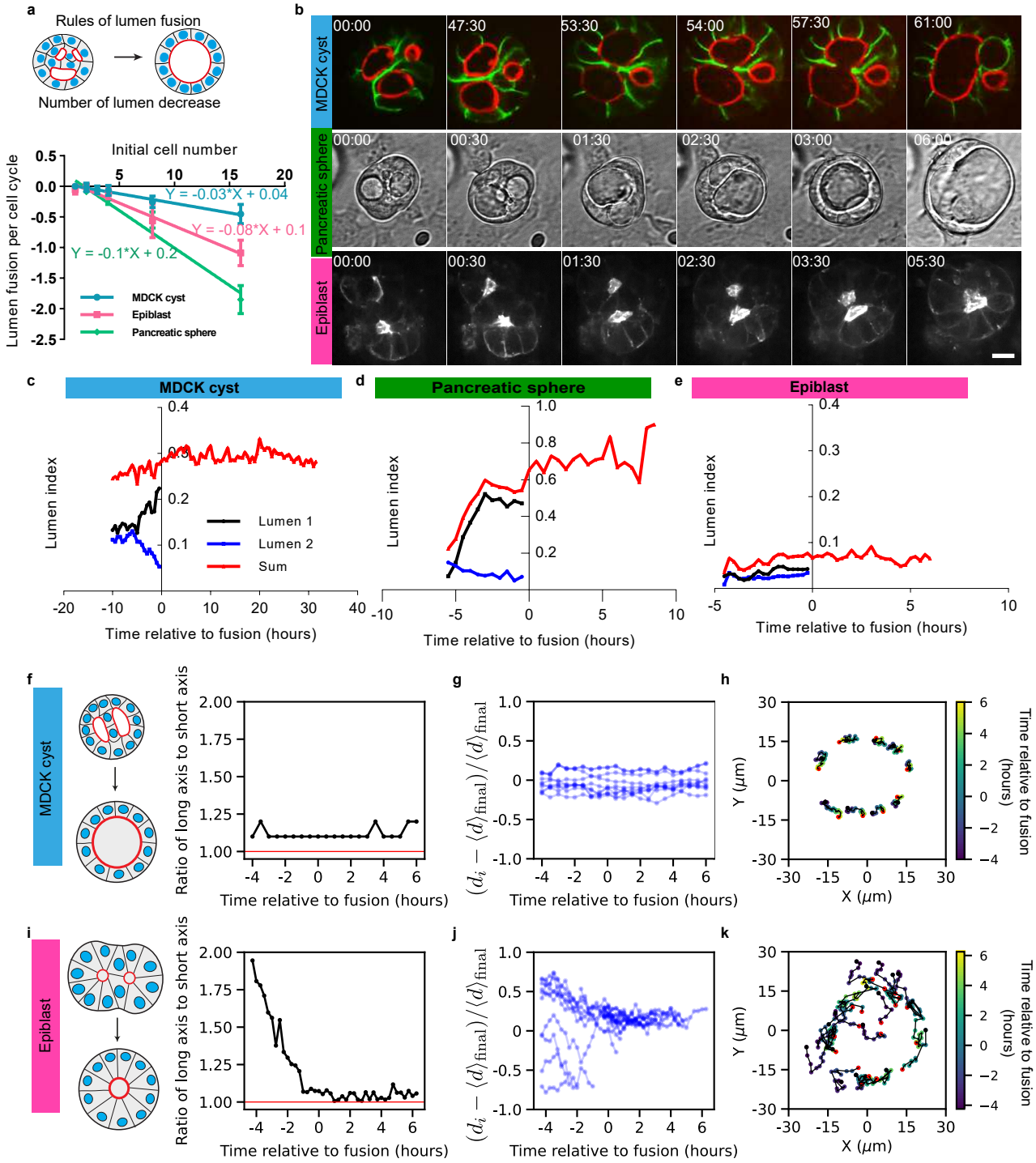

Figure 4 - Rules of lumen fusion in the 3 systems. MDCK and pancreatic spheres lumens fuse by increasing the lumen index whereas epiblasts fuse by cell motion with low lumen index. a. Top: scheme of lumen fusion corresponding to Phase II. Bottom: quantification for the speed of lumen fusion. The plot represents lumen fusion per cell cycle as a function of initial cells number, see Materials and Methods (mean value ± standard error of the mean and the curves represent the fit of mean). Pancreatic spheres and epiblast display faster lumen fusion than MDCK cysts. b. Lumen fusion across systems. Top: MDCK cyst (E-cadherin in green and Podocalyxin in red, also see Movie 5). Middle: Pancreatic sphere (phase contrast images, also see Movie 6). Bottom: epiblast (Sir-actin, also see movie 7). c-e. Comparison between lumen indices (ratio of surface of lumen over the surface of cyst) for the three systems presented on panel b: MDCK cyst (c), pancreatic sphere (d) and epiblast (e). For each system, the blue and black curves correspond to individual lumen 1 and 2 on panel b, note the change in scale in the y-axis. f-l. Characterisation and comparison between cellular dynamics and tissue morphology in MDCK cyst (top) and epiblast (bottom). f,i. Elongations of the cyst defined as the ratio of long axis over short axis of the organoid as a function of time. g,h. Distance between the center of cells and the center of cysts over time. During the fusion process, MDCK cells are at a constant distance from the center of the cyst whereas epiblast cells move inwards. h,l. Single cells trajectories. Time is indicated with color bar and red points indicate the last time point. Epiblast cells display centripetal motion.

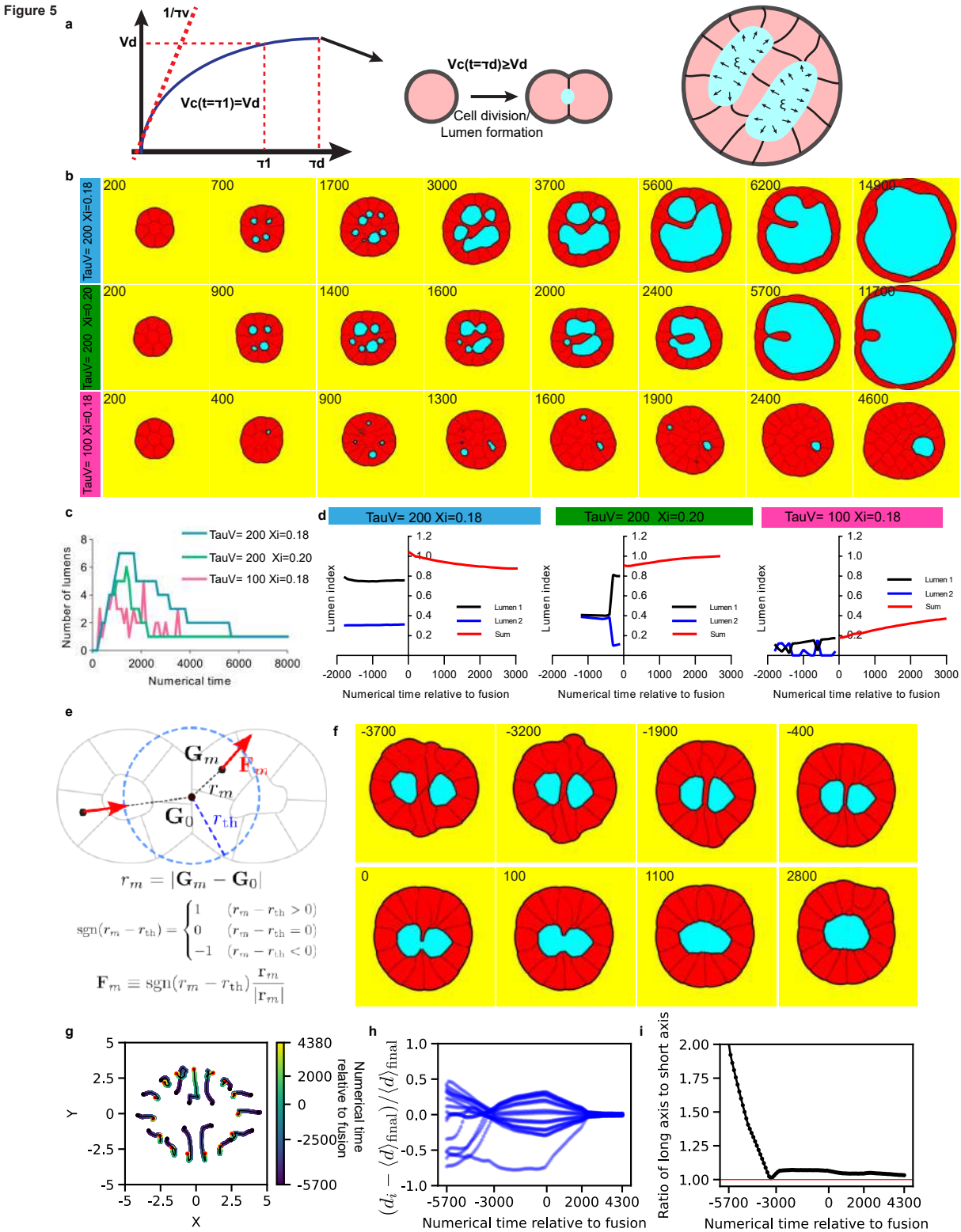

Figure 5 – Numerical simulations of the nucleation and fusion of lumens for the 3 systems based on phase field model. a. The cells increase in volume and divide when they reach a threshold volume or after a threshold time. A lumen is formed after each division. The numerical cysts grow over time; see Movie 8 for typical numerical evolution of cysts. b. The pressure ξ and proliferation time are controlled and three conditions are plotted as a function of time. Each case corresponds qualitatively to each experimental system, see also Movie 9 and Movie 10. c. Quantification of the number of lumens as a function of time. The number of lumens firstly increases and then decreases. These two subsequent phases are similar to the experimental phases reported in Fig. 1 and in Fig. 2. d. Numerical lumen indices measured for the 3 conditions. Their dynamics are similar the 3 experimental dynamics reported in Fig. 4. e-i. Numerical simulations for the fusion of epiblast-like cysts, see also Movie 11. e. Definition of parameters for the fusion of epiblast-like cysts. f. Fusion of two lumens in epiblast-like condition. g-i. The cell motions are tracked (g) as well as the distance of cells with respect to the center of mass of the system (h) and the change in aspect ratio of the cysts (i). The numerical dynamics correspond closely to the experimental time evolution of the same measurements in epiblasts fusion, see Fig. 4j-l.

Figure 6

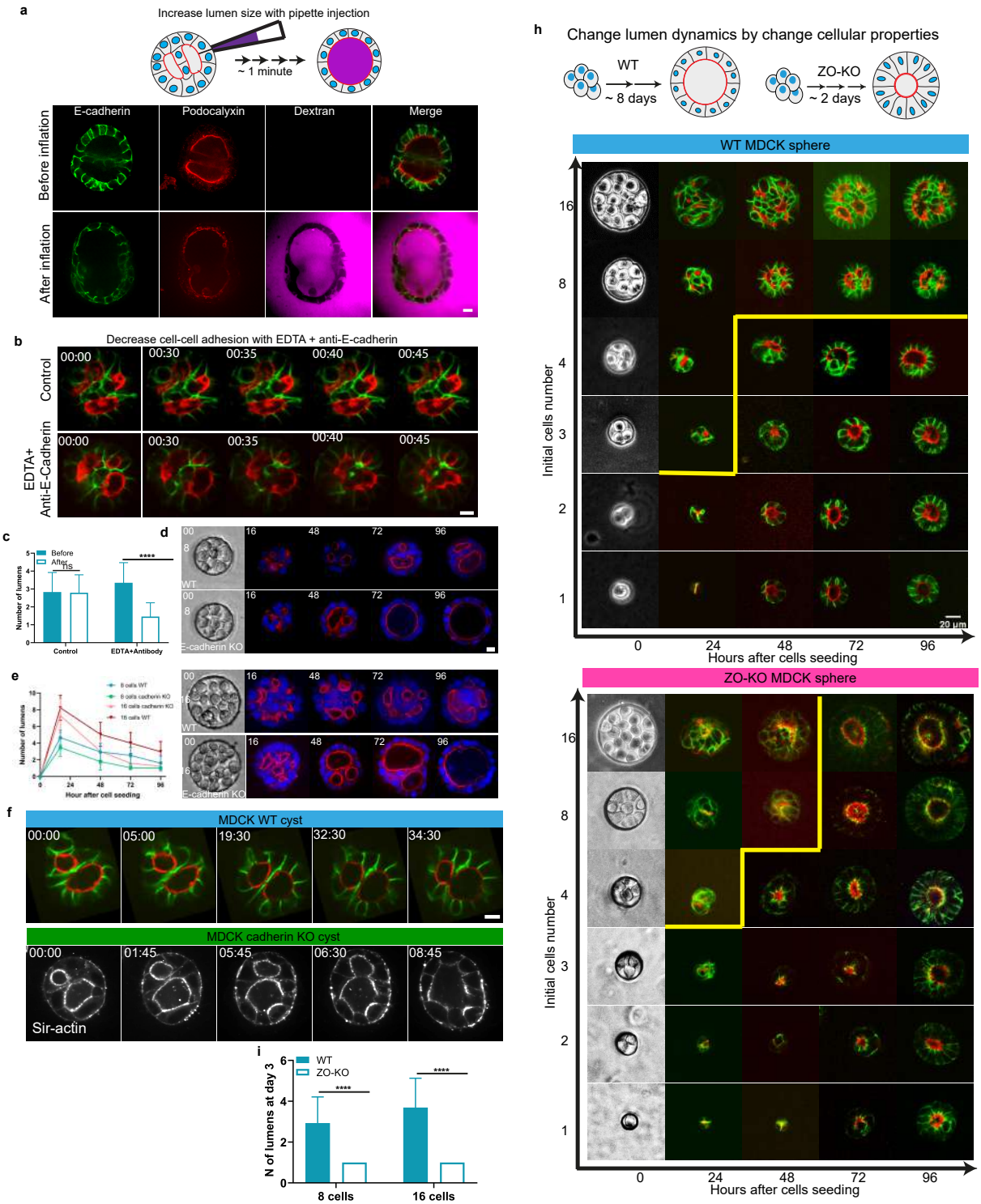

Figure 6 - Testing the fusion mechanisms with perturbation experiments on MDCK cysts. Increasing lumen size by injection or decreasing cells adhesion leads to faster to lumen fusion. a. Inflating MDCK spheres with micropipette. E-cadherin in green and podocalyxin in red and Dextran in Magenta. Scale bar: 10 µm. The inflation triggers the fusion between lumens. b. Decrease in cells adhesion leads to faster lumen fusion. Snapshot of timelapse with control (top) and EDTA + antibody block (bottom). E-cadherin in green and podocalyxin in red. Scale bar: 10 µm. c. Quantification of number of lumens right before and 1 hour after EDTA+antibody treatment. Two independent experiments (n control=15; n EDTA=16). d-f. Decreasing cell adhesion by using MDCK E-cadherin KO. The comparisons between MDCK WT and E-cadherin KO cysts over time and initial cell number in d (top two rows: 8 cells, bottom two rows: 16 cells). e. Quantification of the number of lumens in WT and E-cadherin KO cysts as a function of time for the initial cell number 8 and 16 cells. f. Dynamics of lumen fusion in WT and in E-cadherin KO cysts with 8 cells initial cell number, time in hh:mm. g. ZO-KO cyst have faster lumen fusion than WT in MDCK cysts with controlled initial cell number. Dynamics of MDCK WT cysts (top) and ZO-KO cyst (bottom) with readouts of E-cadherin in green and Podocalyxin in red. The yellow line outlines zones with a single lumen (8 cells WT=15; 16 cells WT=16; 8 cells ZO-KO=13; 16 cells ZO-KO=16). h. Quantification of the number of lumens for the MDCK cysts comparison of panel g at Day 3. Mutant cysts fuse faster. Three independent experiments. Statistical analyses: **** corresponds to $p < 0.0001$.

Figure 7

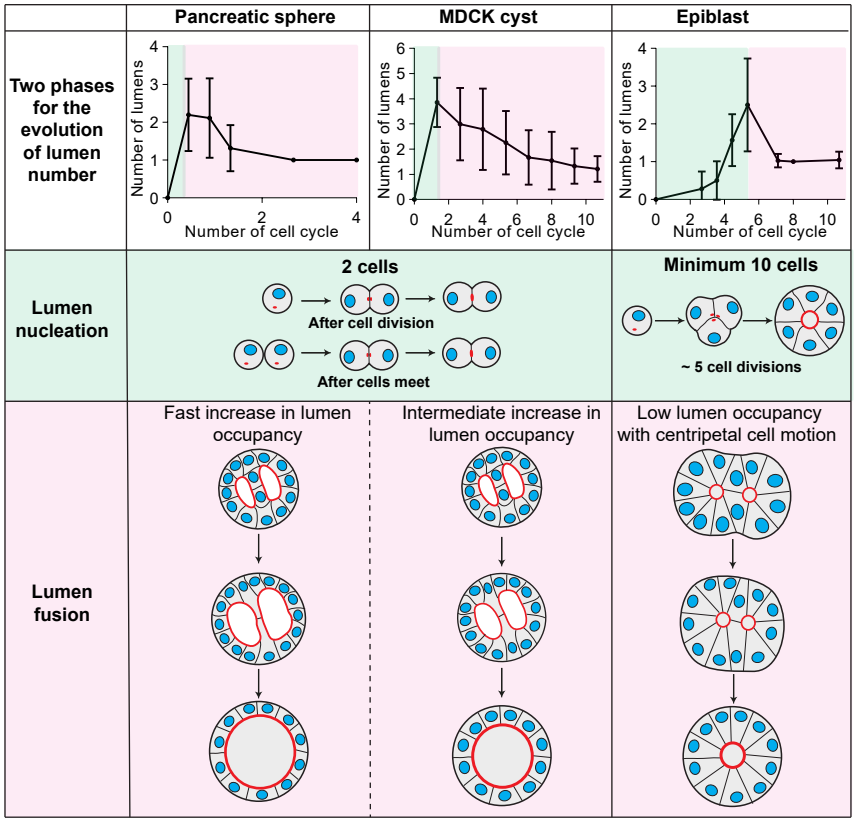

Figure 7 – Generic rules of nucleation and fusion. Row 1 : Pancreatic spheres, MDCK cysts and epiblasts have two phases for the number of lumens as a function of time. **Row 2 :** Nucleation rules are similar for pancreatic spheres and MDCK cysts, lumens form after cell division and when two cells meet; in contrast, a minimum of about 10 cells are required for the lumen nucleation of lumens in epiblasts. **Row 3 :** Lumens fusions are similar between pancreatic spheres and MDCK cysts but with distinct pumping rates. In pancreatic spheres, fast pumping leads the increase in lumen index and subsequent fusion; in MDCK cysts, lower increase in lumen index leads the fusion. In contrast, fusion occurs with centripetal cell motion in epiblasts with low lumen occupancies.

Extended Figure 1

a

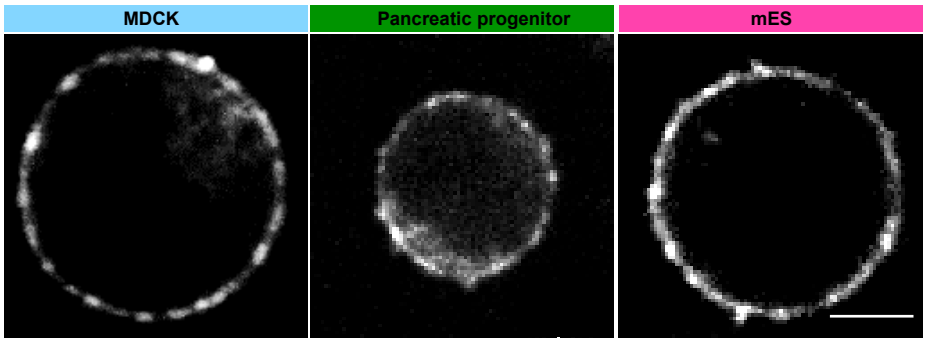

b

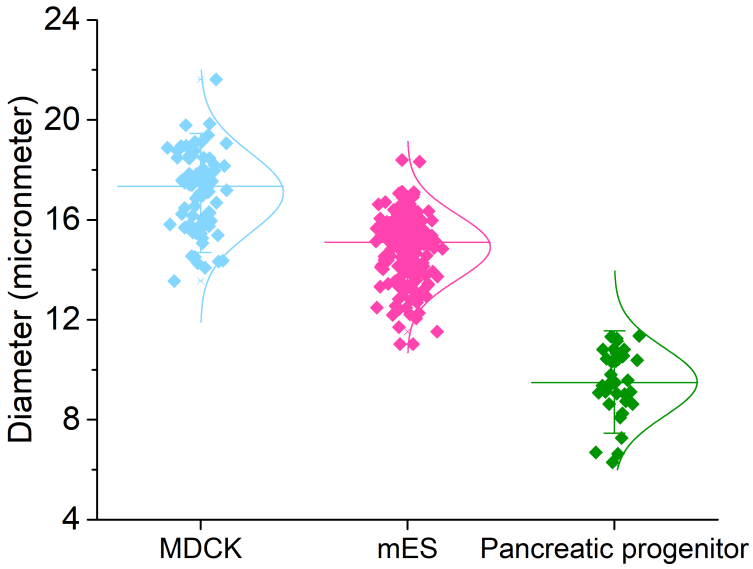

c

Initial cell numbers	MDCK cyst	Pancreatic sphere	Epiblast
	Diameter of cavities (µm)		
1	17.5	10	15
2	25	14	21
3	30	-	-
4	35	20	30
8	50	30	42
16	70	40	60

Extended Figure 1: Diameter measurement. a. Middle plane of single cells for MDCK, mES, pancreatic progenitor from top to bottom labeled with Sir-actin. b. Diameter distribution: N=3, n(MDCK)=75, n(mES)=202, n(pancreatic progenitor)=35. Scale bar 5 µm. c. Selections of diameters for cavities for distinct cells.

Extended Figure 2

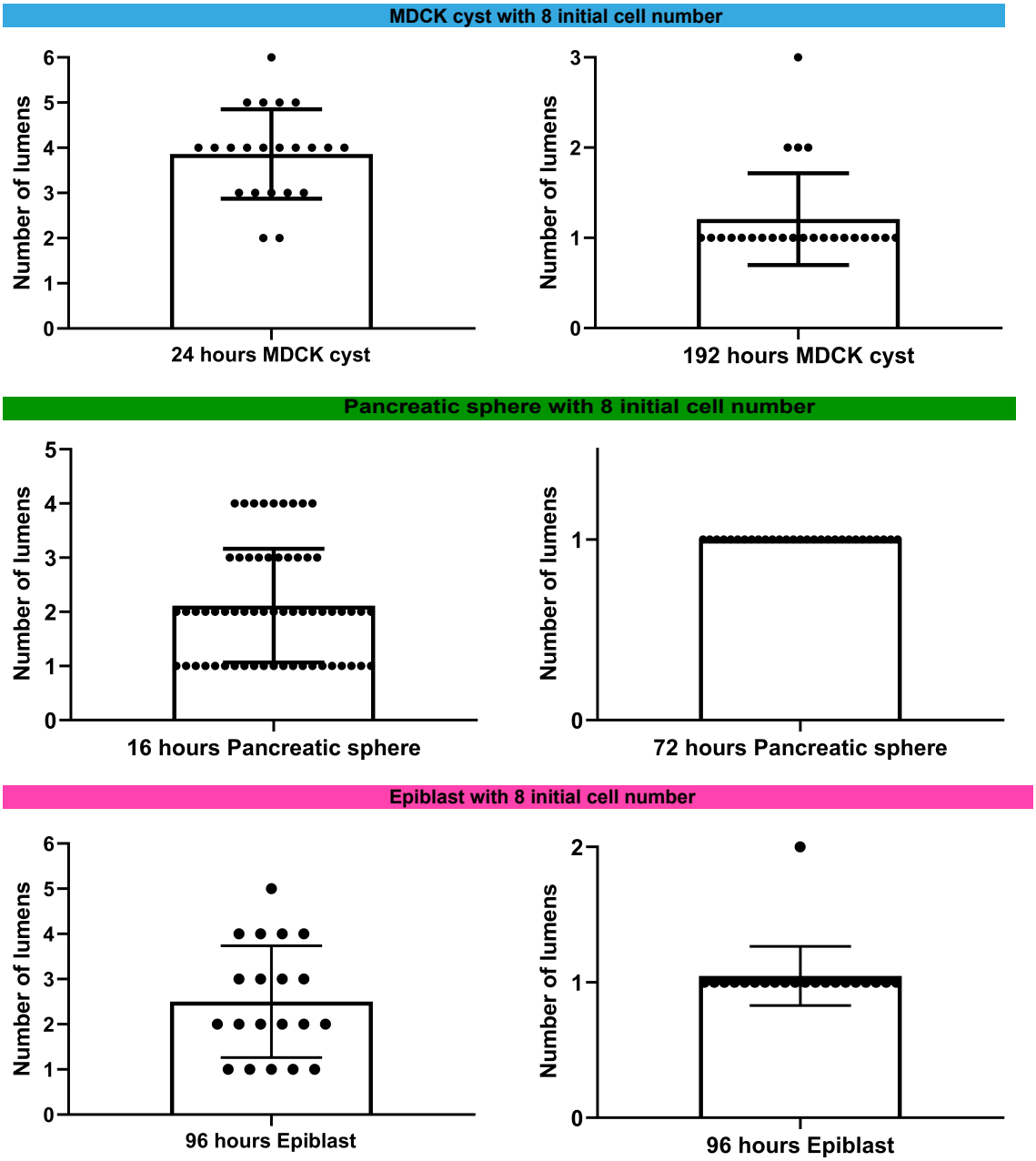

Extended Figure 2: Examples of distributions for the number of lumens at the peak value at the end of Phase I (Left) and at the end of Phase II at the single lumen stage (Right).

Extended Figure 3

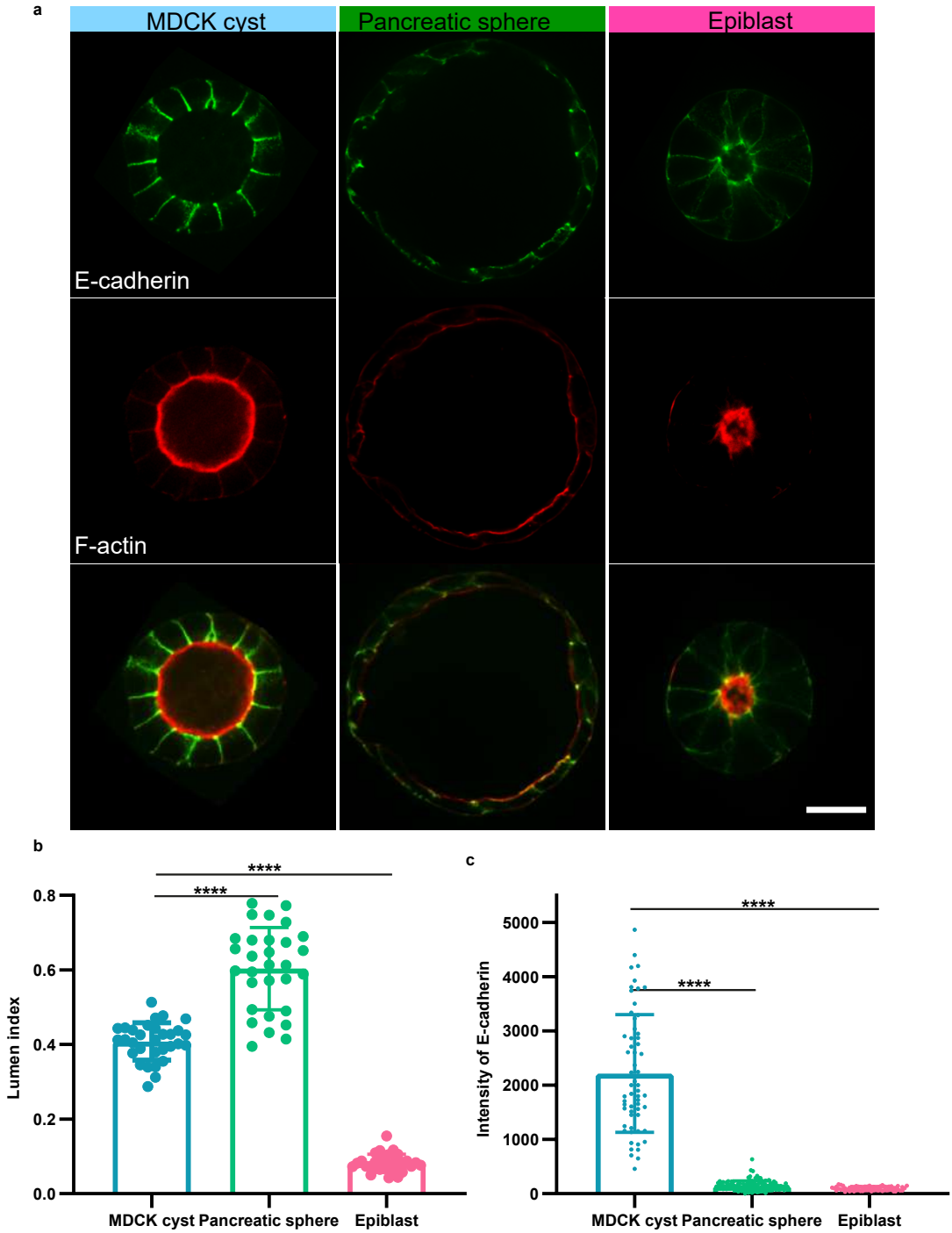

Extended Figure 3: Comparison between the phenotypes in MDCK cysts, pancreatic spheres and epiblasts. a. Typical images of the 3 systems with readouts for E-cadherin in green and F-actin in red. Scale bar 10 µm. b. Quantification of lumens index for three systems. c. Comparison of E-cadherin levels between the 3 systems defined as intensity of E-cadherin on the junction minus intensity in the cytoplasm and normalised by the intensity of the background. **** corresponds to $p < 0.0001$.

Extended Figure 4

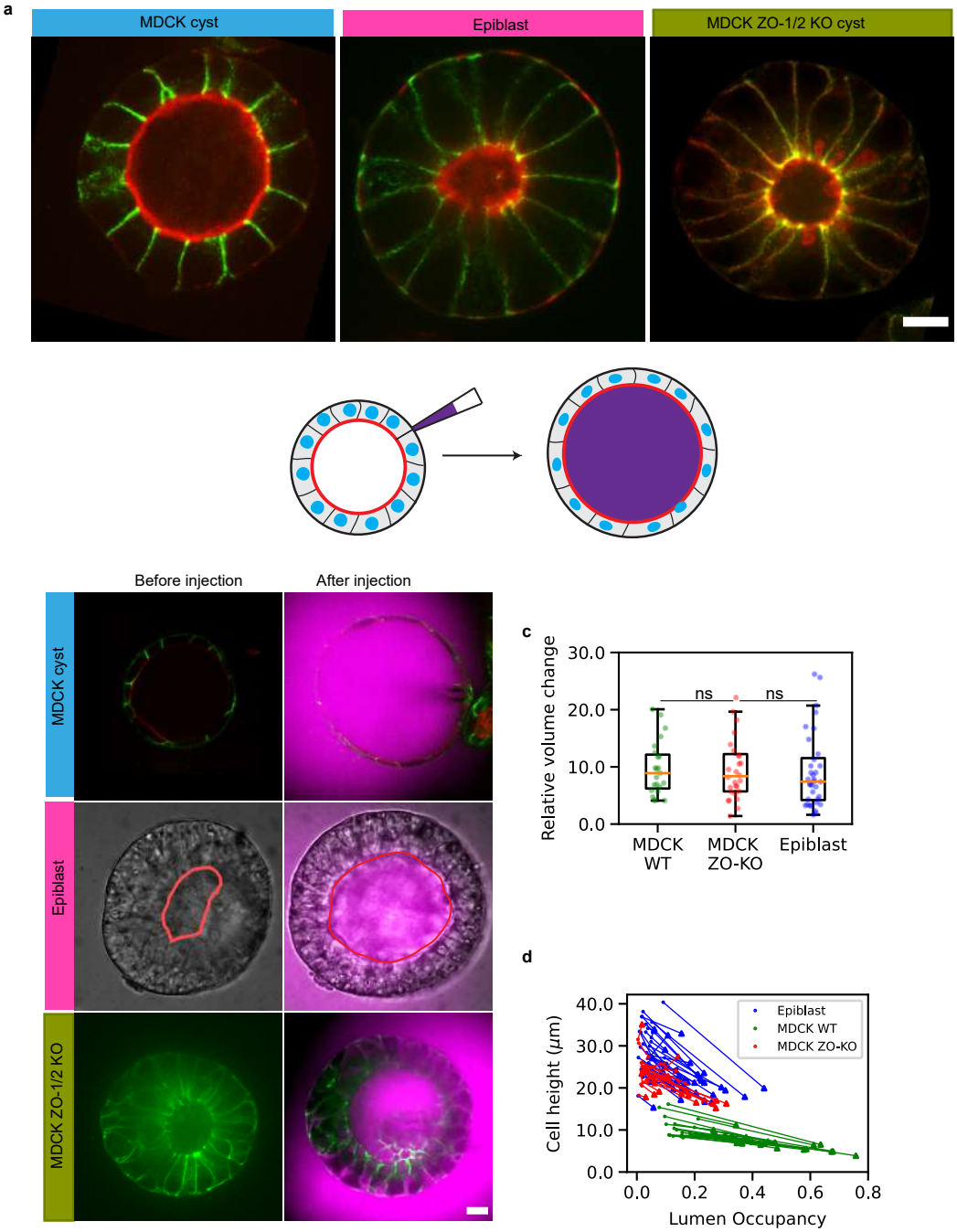

Extended Figure 4: Comparison between MDCK wild type, ZO1/ZO2 KO cysts and epiblasts. a. Cell-cell contacts and lumens are stained with E-cadherin (in green) and F-actin (in red), scale bar: 5 µm. Note the low lumen index in epiblasts and in MDCK ZO1/ZO2 KO cysts. b-d. Comparison between inflation response. b. Images are shown before and after inflation. c. Change fold in the lumen volume for each system, statistical test. d. Change in cell height for each system[21]. ns indicates non-significant P value >0.05.